Electronic Supplementary Material (ESI) for Nanoscale.

Nanocrystal Heterostructures of $LiCoO_2$ with Conformal Passivating Shells

Bob Jin Kwon[a], Patrick J. Phillips[b], Baris Key[c], Fulya Dogan[c], John W. Freeland[d], Chunjoong Kim[a,e], Robert F. Klie[b] and Jordi Cabana[a]*

[a]Department of Chemistry, University of Illinois at Chicago, Chicago, IL 60607, United States

[b]Department of Physics, University of Illinois at Chicago, Chicago, IL 60607, United States

[c]Chemical Sciences and Engineering Division Argonne National Laboratory Argonne, IL 60439, United States

[d]X-ray Science Division, Advanced Photon Source, Argonne National Laboratory, Argonne, IL 60439, USA

[e]School of Materials Science and Engineering, Chungnam National University, Daejeon, 305-764, Republic of Korea

Supplementary information

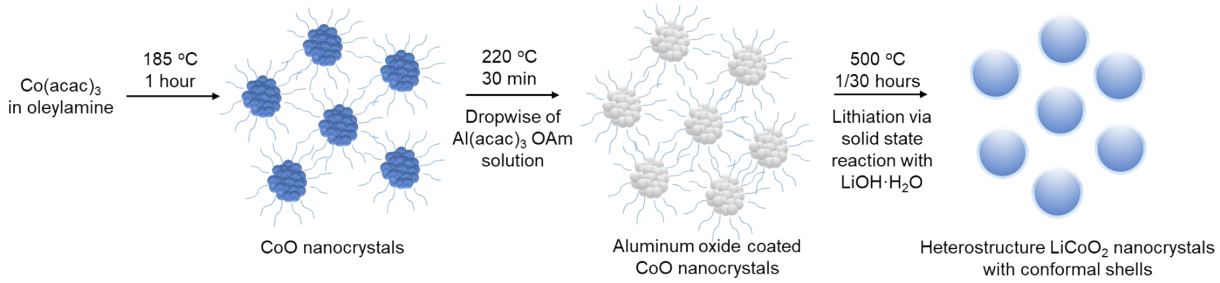

Figure S1. A scheme for the preparation of heterostructure $LiCoO_2$ nanocrystals with conformal shells.

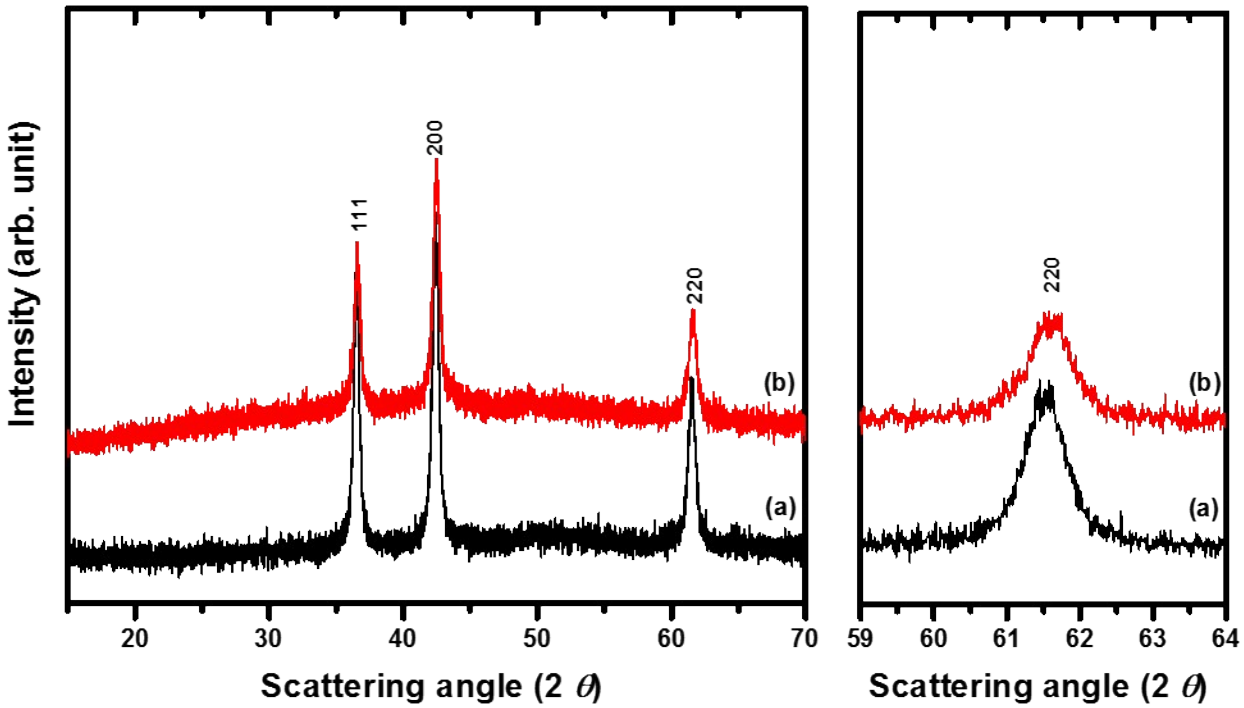

Figure S2. X-ray diffraction patterns of (a) CoO and (b) core-shell CoO nanocrystals.

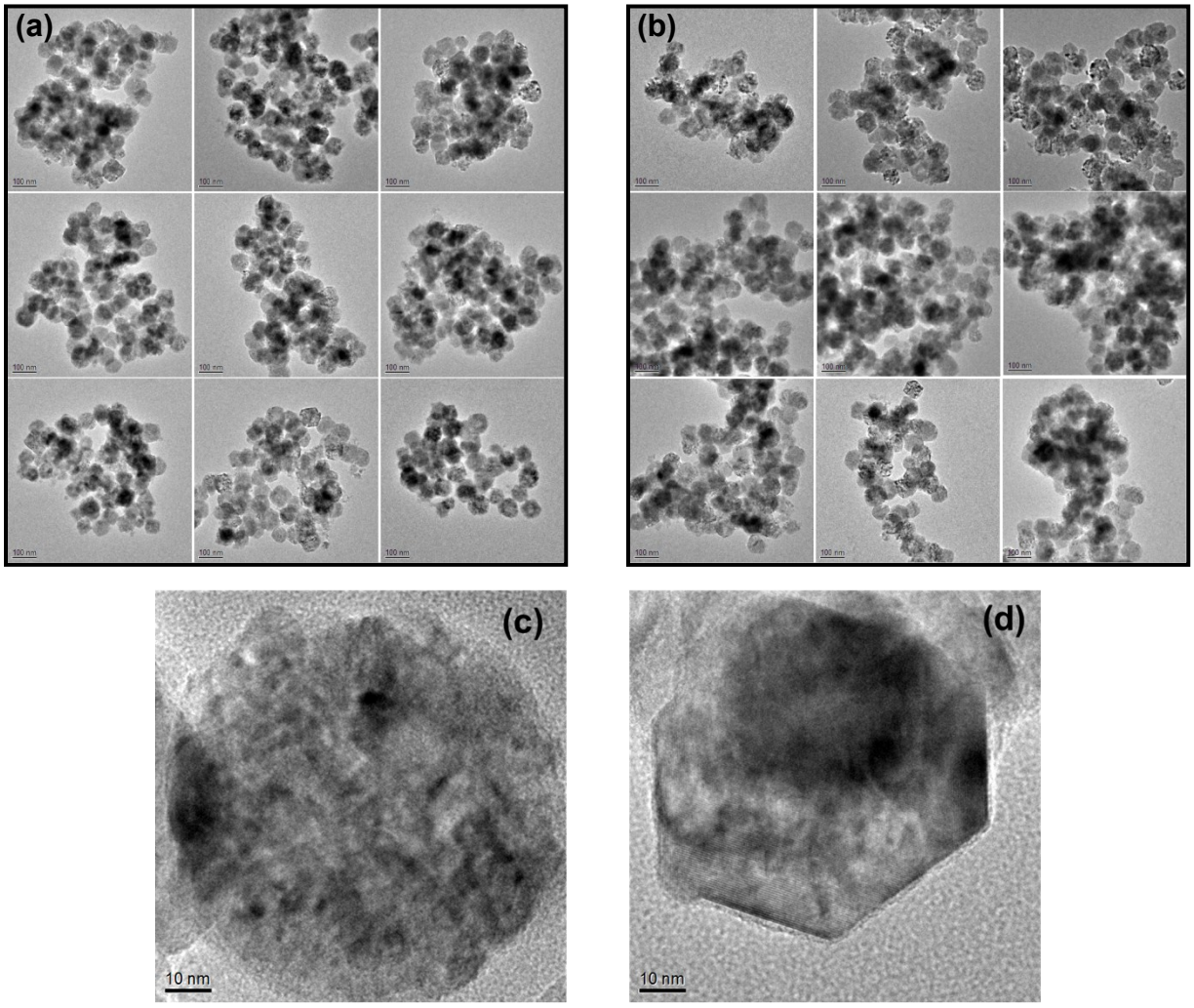

Figure S3. TEM images of (a) $LiCoO_2$-1h and (b) $LiCoO_2$-30h nanocrystals used to measure the populations with spherical or platelet morphology. Representative TEM images of spherical (c) and faceted (plate-like) (d) morphologies in the $LiCoO_2$ nanocrystals.

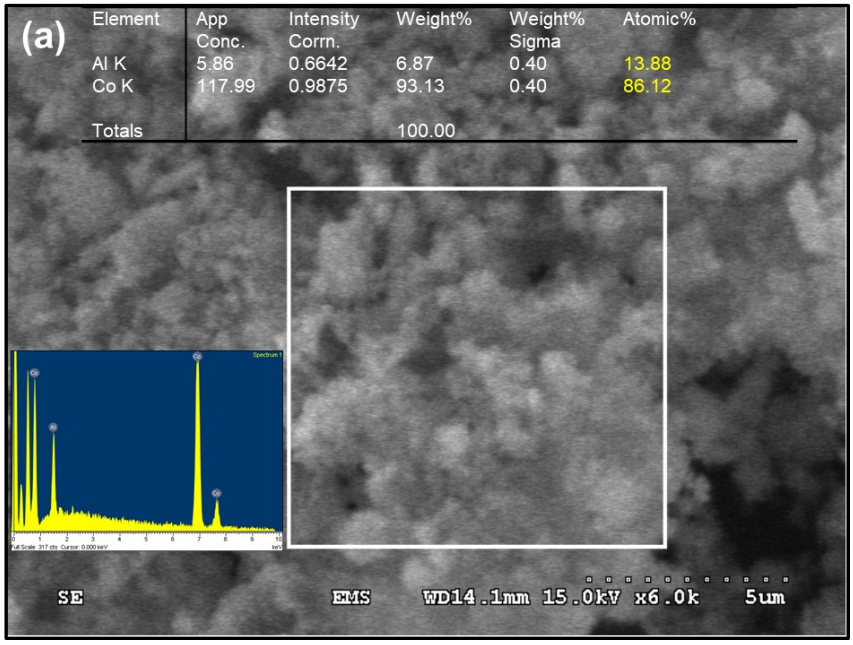

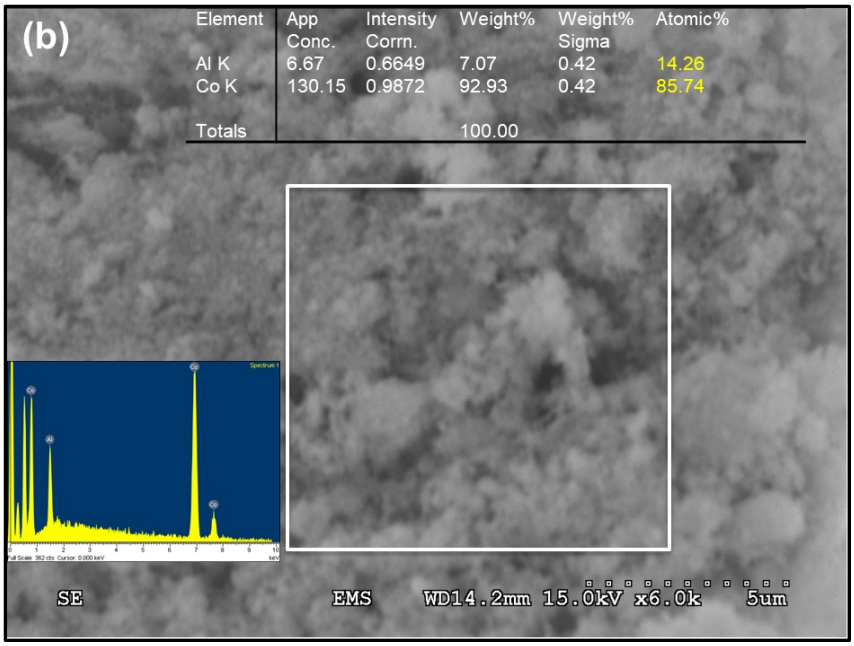

Figure S4. SEM image and corresponding EDX spectrum of (a) CS-$LiCoO_2$-1h and (b) CS-$LiCoO_2$-30h nanocrystals.

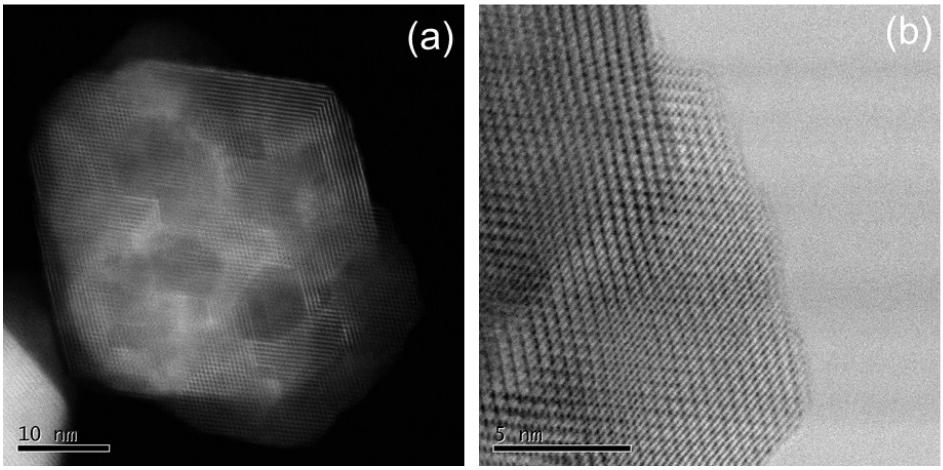

Figure S5. (a) LAADF and (b) ABF images of CS-$LiCoO_2$-30h nanocrystals

	Charge capacity above 3.9 V (mAh/g)	Charge capacity below 3.9 V (mAh/g)	% capacity of LT
LCO 1h	***84.1 ± 0.3***	***59.6 ± 2.1***	***41.5 ± 0.8***
CS-LCO 1h	***70.6 ± 1.4***	***41.4 ± 2.6***	***36.9 ± 1.7***
LCO 30h	***93.6 ± 1.8***	***58.6 ± 3.7***	***38.5 ±1.6***
CS-LCO 30h	***73.4 ± 0.4***	***49.3 ± 0.8***	***40.2 ±0.3***

Table S1. Specific capacities below and above 3.9 V during the first charge. These values are considered qualitatively representative of the ratio of HT- and LT-phase in the nanocrystals. Percent capacities of LT-phase were calculated as (LT*100/(HT+LT)). All values were taken by averaging three cells.

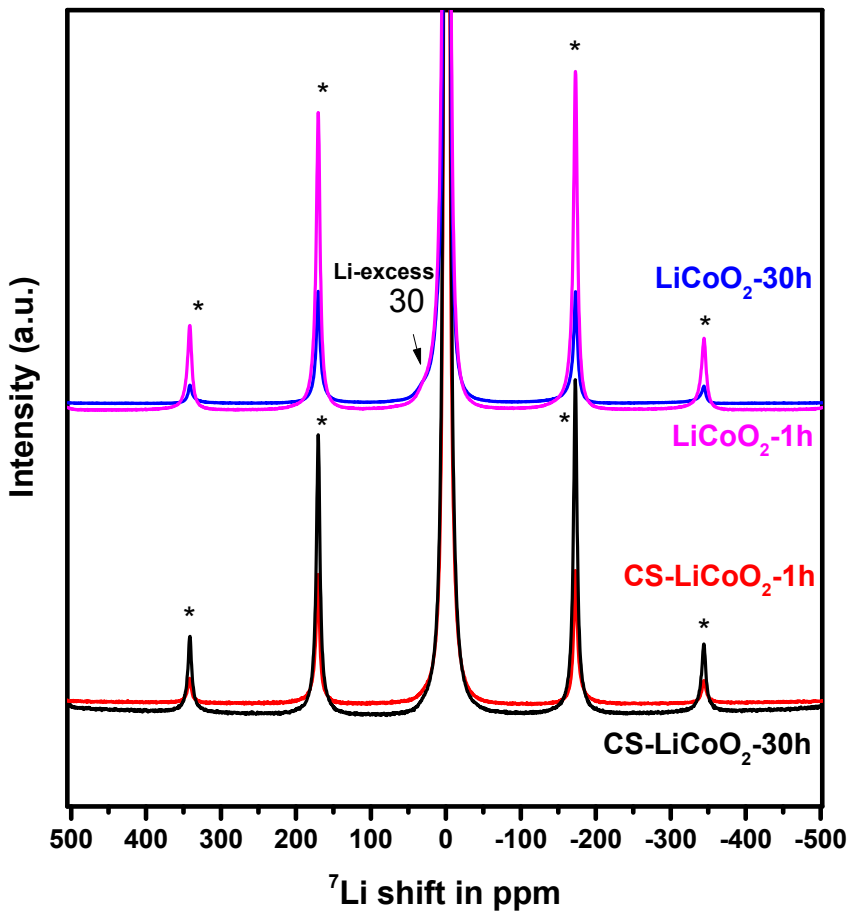

Figure S6. Alternate view of the ^{7}Li MAS NMR spectra of bare and core shell $LiCoO_2$, presented in the manuscript.

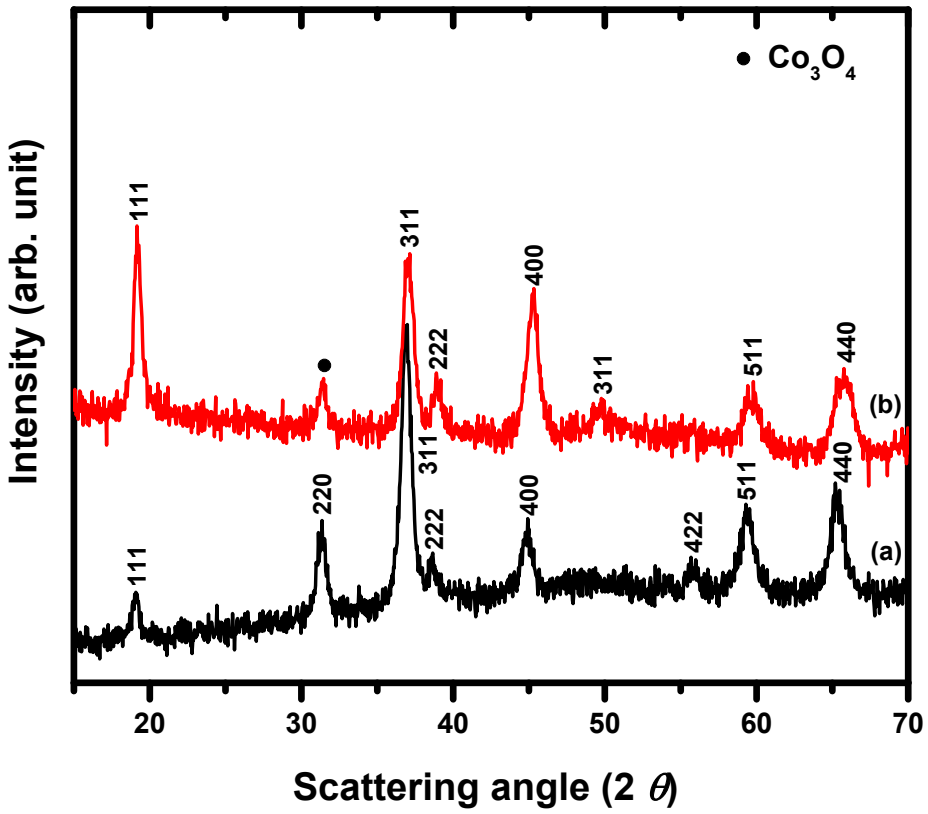

Figure S7. XRD patterns of (a) Co_3O_4 prepared by calcination of CoO nanocrystals at 300 ^oC for 4 hours and (b) spinel $LiCoO_2$ nanocrystals.

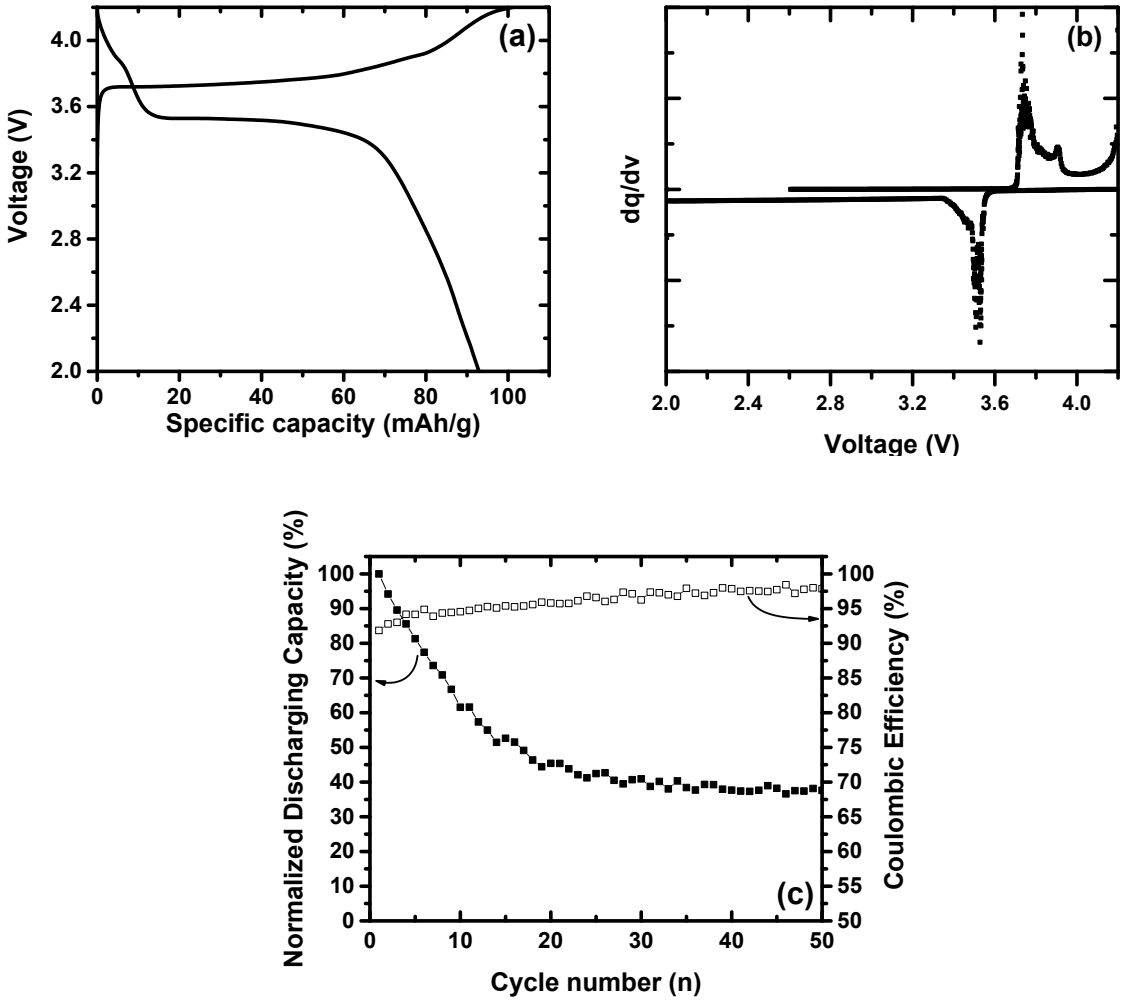

Figure S8. (a) Voltage versus specific capacity profiles, (b) corresponding *d*Q/*d*V plots of spinel $LiCoO_2$ nanocrystals (Figure S5) and (c) evolution of normalized specific capacity (solid symbol) and Coulombic efficiency (open symbol) when cycling with a discharge cutoff voltage of 2.0 V and a charge cutoff voltage of 4.2 V vs Li^+/Li^0 at C/20 rate.

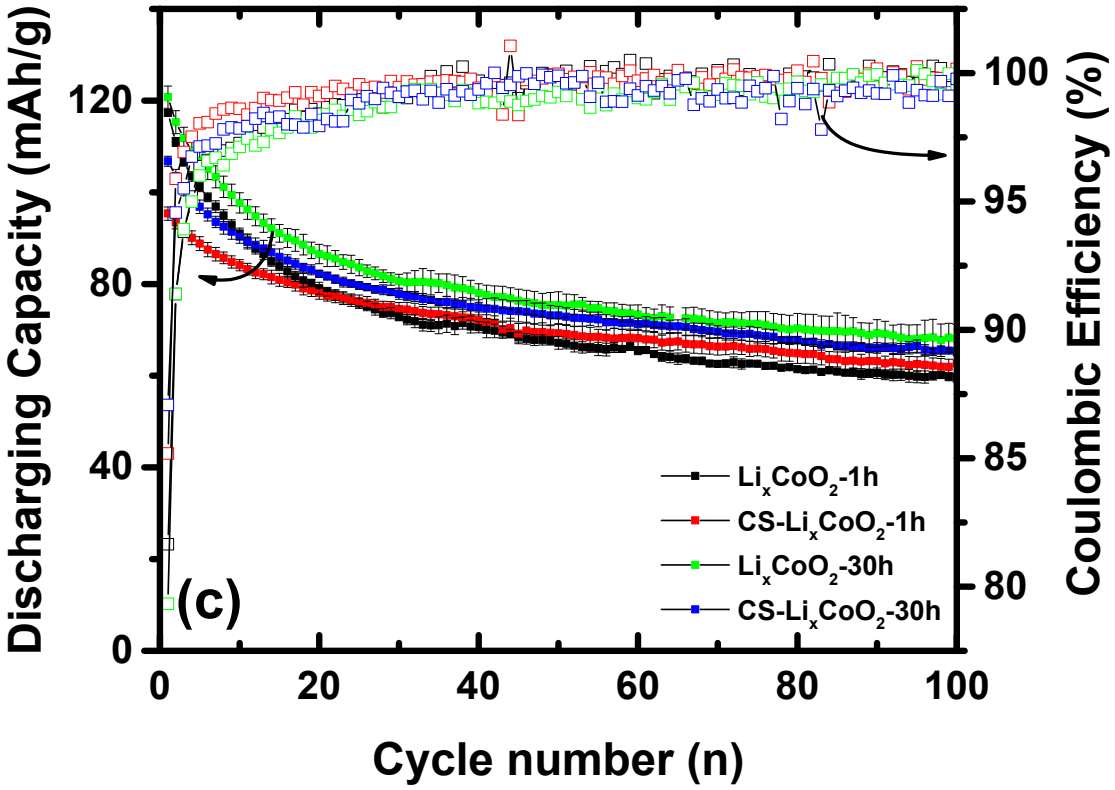

Figure S9. Evolution of discharging specific capacity (solid symbol) and Coulombic efficiency (open symbol) when cycling at C/20.

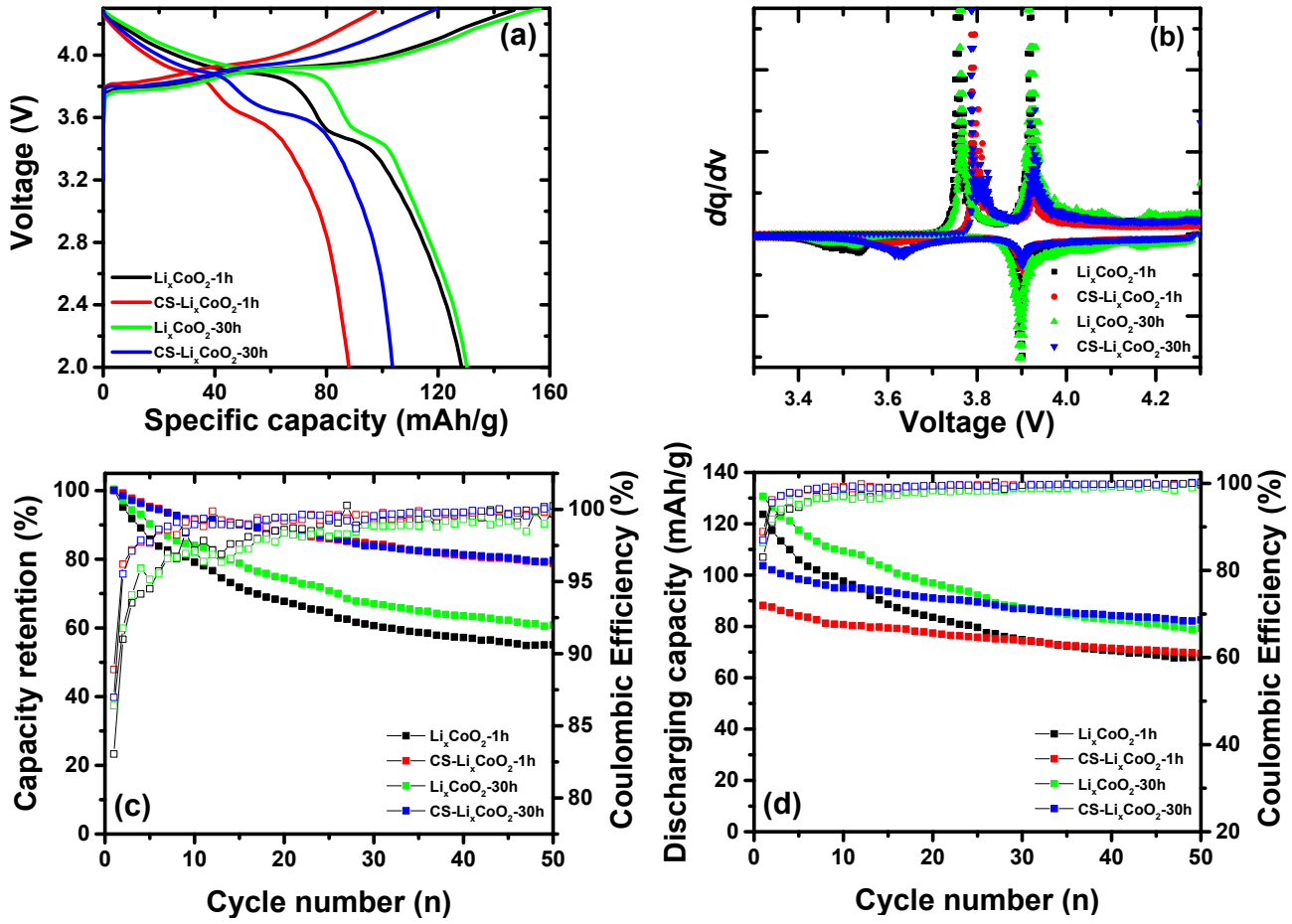

Figure S10. (a) Voltage versus specific profiles, (b) corresponding *d*Q/*d*V plots, (c) normalized specific capacity (solid symbol) and coulombic efficiency (open symbol), and (d) absolute discharge capacity (solid symbol) and coulombic efficiency of bare and core-shell $LiCoO_2$ nanocrystal electrodes when cycled at C/20 in an electrolyte consisting of 1.2 M $LiPF_6$ in a 3:7, w/w, mixture of ethylene carbonate (EC) and ethyl methyl carbonate (EMC).

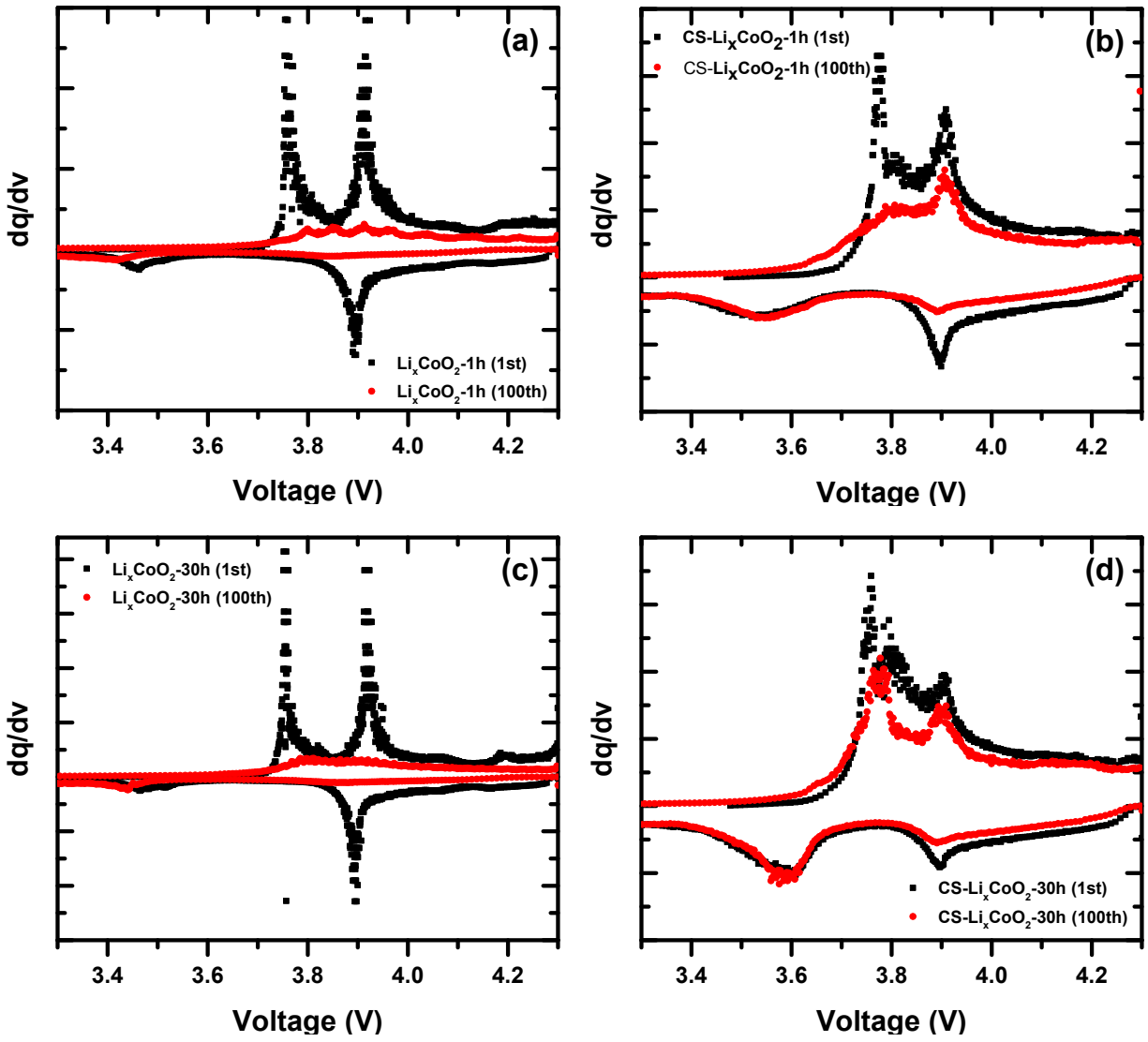

Figure S11. *d*Q/*d*V plots of (a) $LiCoO_2$-1h, (b) CS-$LiCoO_2$-1h, (c) CS-$LiCoO_2$-30h, and (d) CS-$LiCoO_2$-30h in the 1st (black) and 100th cycle (red), corresponding to the cells in Figure 6.